ACCURATE DELINEATION OF IMPACT CRATERS BY IMAGE ANALYSIS. P. Pina[1] and J. S. Marques[2], [1]CERENA, Instituto Superior Técnico, Av. Rovisco Pais 1049-001, Lisboa, Portugal (ppina@ist.utl.pt), [2]ISR, Instituto Superior Técnico, Av. Rovisco Pais 1049-001, Lisboa, Portugal (jsm@isr.ist.utl.pt).

Introduction: The very high resolution of the cameras on-board current planetary probes is permitting to indubitably unveil an astronomical amount of craters, never perceived before. This has naturally pushed the development of CDA-crater detection algorithms [1-3]. Their adaptive nature permits achieving a high level of robustness in different surfaces and consequently becoming an important tool in the update of crater catalogues [4-5]. Nevertheless, the available CDA assume all craters as circular and only provide as output the radius and location of each crater. The local evaluation of the craters rims (degradation or preservation status) is an important issue, for instance, to analyse past climates [6-7]. The automated delineation has been seldom addressed [8] and not in a systematic way. At this stage, where the problem remains wide open and where different trends can be evaluated, we start our research on the subject by presenting two independent solutions for the delineation of craters: one that processes crater images in polar coordinates (designated by 'Polar'), the other based on mathematical morphology ('Morphological'). Both methods use a-priori information about the location and size of each crater.

'Polar' Method: This solution is built on 2 phases (details can be consulted in [9]):

(i) *Coarse estimation of the crater boundary* - This step aims to approximate the crater boundary by a circle. The crater image is first filtered using a lowpass filter (Gaussian) to smooth it and reduce noise. Then, it is transformed to a new coordinate system (polar coordinates), where the crater boundary becomes an horizontal line, which can be automatically estimated. In a crater image we observe that on one half we have a transition from shadow to illuminated points when we move out of the crater, while in the other half of the crater we observe the opposite. To compensate this change of illumination we subtract points with the same distance to the crater center and with angles separated by 180º. By integrating the image along the a given direction, an intensity profile is obtained: the crater radius is defined as the point of highest negative slope after the global maximimum point (Fig. 2b and 2c).

(ii) *Detailed boundary estimation* – The previous step is an attention mechanism that permits focusing in a much smaller space region. The intensity transitions along vertical lines of the polar image are detected using a Sobel mask for vertical transitions. Then, the connected components are extracted leading to a set of segments (Fig. 1d). Small segments and segments outside the region of interest are discarded (Fig. 1e). Then, overlapping segments along the vertical direction are detected and the smaller one removed, obtaining a set of reliable segments which do not overlap. A linear interpolation permits to fill the gaps between neighboring segments (Fig. 1f, bottom row shows the output of each step in Cartesian coordinates).

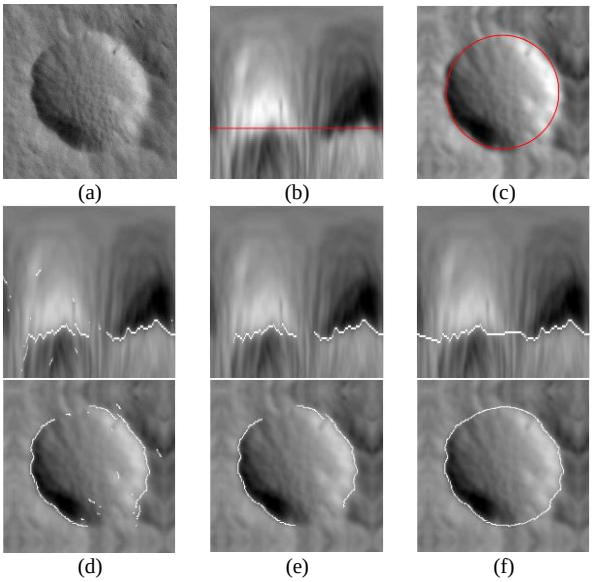

Fig. 1. Polar method: (a) Initial image (crater diameter is 48m); (b) Filtered image in polar coordinates and estimated coarse contour (red line); (c) The same as (b) in Cartesian coordinates; (d) Detection of vertical intensity transitions; (e) Filtering of segments outside the region of interest; (f) Final contour. [image credits: NASA/JPL/Univ. Arizona]

'Morphological' Method: This algorithm is built in 2 main phases (consult [10] for the details):

i) *Filtering with connected operators* – This preprocessing uses two morphological filters, opening and closing by reconstruction [11], whose main issue is to filter out some components while perfectly preserving the contours of the remaining ones. These operators remove basins (peaks) of the image whose depth (height) are smaller than a given contrast *h*. They are sequentially applied on the crater images (Fig. 2a), first, by supression of low depth basins (closing by reconstruction) corresponding to small depressions on the terrains or shades of boulders, next, by the removal of low height peaks (opening by reconstruction), producing a simplified image where the countours of relevant information (crater rims) are kept unchanged (Fig.

2b). The intensity of the gradient (Fig. 2c), which will be used in the next phase, also highlights these matters. *(ii) Segmentation by watershed* - The watershed transform, which is based on the analogy of the flooding of a topographic surface from its minima, is used to delineate each crater. The imposition of interesting minima (one internal and one external marker) from which the flooding will start is a crucial point for obtaining a correct delineation. The crater detected by a CDA is the basis to create this pair of markers, the internal by its erosion and the external by the contour of its dilation (Fig. 2d). The imposition of these minima results in modifying the homotopy of the image, that is, in changing their number of extrema and relative locations [12]. After that, the watershed transform is applied with the guarantee that always only one single closed contour is delineated between the markers (Fig 2e-f).

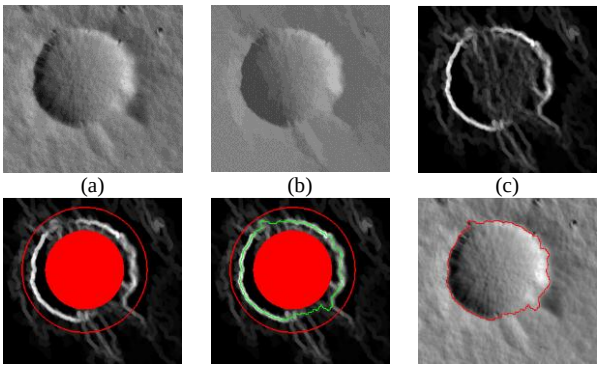

Fig. 2. Morphological method: (a) Initial image (crater diameter is 35 metres); (b) Filtered; (c) Gradient; (d) Markers over gradient image; (e) Delineated contour (green) between markers; (f) Delineated contour over initial image. [image credits: NASA/JPL/Univ. Arizona]

Experimental Results: The algorithms were evaluated using a dataset of 60 crater images of the same HiRISE image (ESP-011491-2090). We selected 30 well preserved craters (contour clearly visible without interruption) and 30 modified craters (missing or poorly defined contour in some regions). The craters vary from 9 to 722 m in diameter. Accurate contour estimates are obtained in the case of preserved craters by both methods. In the case of modified craters, there is less information available and the contour estimates are based on the interpolation in large segments of the crater rim. This leads to less natural and smooth curve segments. The algorithms were also evaluated by comparing the contour estimates with manually created ground truth contours with a metrics proposed in [13]. We assume that the detected contour should be within a band of a given width around the ground truth contour. Points outside this band are considered errors and their proportion used as a distortion measure between both contours. The performances shown in table 1 and Fig. 3 can be considered very good and independent from the size of the craters.

Table 1. Delineation performances in % for Polar (P) and Morphological (M) methods (dc-delineated contours, cp-detected crater points).

	Preserved Craters			Modified Craters		
	dc	cp	errors	dc	cp	errors
P	100.0	97.7	2.3	60.0	91.3	8.7
M	100.0	95.9	4.1	100.0	89.9	10.1

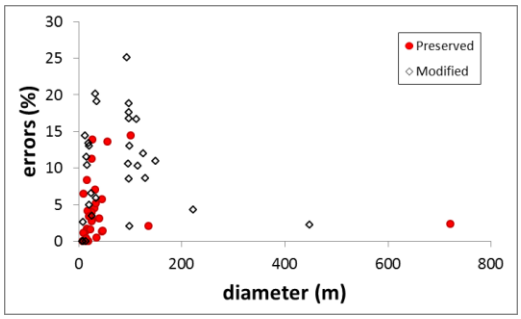

Fig. 3. Plot of errors vs. craters diameter.

Conclusions: These algorithms are adequate to deal with the delineation of impact craters in images of centimetric resolution, since they are able to estimate precise crater contours with high performances. The Polar method leads to detections with smaller errors, but the Morphological algorithm can estimate a contour in every crater. Future improvements include the combination of both algorithms, so to quantify the degradation/preservation status and propose an individual index. Additional work will also include the testing of this approach on other regions of Mars, as well as, other teluric surfaces as Mercury, the Moon and Phobos.

Acknowledgements: Work developed in the frame of projects PTDC/CTE-SPA/110909/2009 (ANIMAR) and PEst-OE/EEI/LA0009/2011 (ISR), both funded by FCT-Portuguese Science Foundation.

References: [1] Bandeira L. et al. (2007) IEEE TGRS, 45, 4008-4015. [2] Martins R. et al. (2009) IEEE GRSL, 6, 127-131. [3] Urbach E. and Stepinski T. (2009) PSS, 57, 880-887. [4] Salamunicar G. et al. (2011) PSS, 59, 111-131. [5] Salamuniccar G. et al (2011) Proc. ISPA, 591-596. [6] Mangold N. et al. (2012) JGR, 117, E04003. [7] Watters W. et al. (2011) Icarus, 211, 472-497. [8] Barata T. et al. (2004) LNCS 3212, 489-496. [9] Marques J. S. et al. (2013) IbPRIA, submitted. [10] Pina P. et al. (2013) ICIAR, submitted. [11] Soille P. (2003) *Morphological Image Analysis*, Springer. [12] Beucher S. and Meyer (1993) In *Mathematical Morphology in Image Processing*, ch. 12, 433-481, Marcel Dekker. [13] Grauman K. et al. (2004) Proc. CVPR, 220-227.